# **Recurrent Scale Approximation for Object Detection in CNN**

Yu Liu<sup>1,2</sup>, Hongyang Li<sup>2</sup>, Junjie Yan<sup>1</sup>, Fangyin Wei<sup>1</sup>, Xiaogang Wang<sup>2</sup>, Xiaoou Tang<sup>2</sup>

<sup>1</sup>SenseTime Group Limited

# <sup>2</sup>Multimedia Laboratory at The Chinese University of Hong Kong

liuyuisanai@gmail.com, {yangli,xgwang}@ee.cuhk.edu.hk, {yanjunjie,weifangyin}@sensetime.com, xtang@ie.cuhk.edu.hk

### **Abstract**

Since convolutional neural network (CNN) lacks an inherent mechanism to handle large scale variations, we always need to compute feature maps multiple times for multiscale object detection, which has the bottleneck of computational cost in practice. To address this, we devise a recurrent scale approximation (RSA) to compute feature map once only, and only through this map can we approximate the rest maps on other levels. At the core of RSA is the recursive rolling out mechanism: given an initial map on a particular scale, it generates the prediction on a smaller scale that is half the size of input. To further increase efficiency and accuracy, we (a): design a scale-forecast network to globally predict potential scales in the image since there is no need to compute maps on all levels of the pyramid. (b): propose a landmark retracing network (LRN) to retrace back locations of the regressed landmarks and generate a confidence score for each landmark; LRN can effectively alleviate false positives due to the accumulated error in RSA. The whole system could be trained end-to-end in a unified CNN framework. Experiments demonstrate that our proposed algorithm is superior against state-of-the-arts on face detection benchmarks and achieves comparable results for generic proposal generation. The source code of our system is available. 1.

### 1. Introduction

Object detection is one of the most important tasks in computer vision. The convolutional neural network (C-NN) based approaches have been widely applied in object detection and recognition with promising performance [10, 13, 15, 18, 22, 23, 27, 34, 36]. To localize objects which have arbitrary scales and locations in an image, we

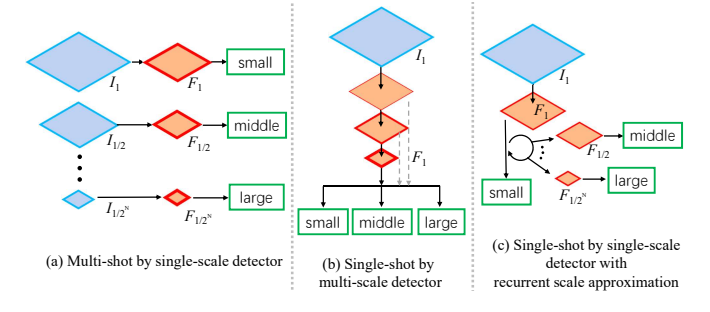


Figure 1. Different detection pipelines. (a) Image pyramid is generated for multi-scale test. Detector only handles a specific range of scale. (b) Image forwarded once in one scale and the detector generates all results. (c) Our proposed RSA framework. Image forwarded once only and feature maps for different scales are approximated by a recurrent unit. Blue plates indicate images in different scale and orange ones with red boarder indicate CNN feature maps in different levels.

need to handle the variations caused by appearance, location and scale. Most of the appearance variations can now be handled in CNN, benefiting from the invariance property from convolution and pooling operations. The location variations can be naturally solved via sliding window, which can be efficiently incorporated into CNN in a fully convolutional manner. However, CNN itself does not have an inherent mechanism to handle the scale variations.

The scale problem is often addressed via two ways, namely, multi-shot by single-scale detector and single-shot by multi-scale detector. The first way, as shown in Fig. 1(a), handles objects of different scales independently by resizing the input into different scales and then forwarding the resized images multiple times for detection [2, 16, 28]. Models in such a philosophy probably have the highest recall as long as the sampling of scales is dense enough, but they suffer from high computation cost and more false positives. The second way, as depicted in Fig. 1(b), forwards the image only once and then directly regresses objects in multiple

 $<sup>^1</sup>Our\ codes$  and annotations mentioned in Sec.4.1 can be accessed at github.com/sciencefans/RSA-for-object-detection

scales [21, 26, 27]. Such a scheme takes the scale variation as a black box. Although more parameters and complex structures would improve the performance, the spirit of direct regression still has limitations in real-time applications, for example in face detection, the size of faces can vary from  $20 \times 20$  to  $1920 \times 1080$ .

To handle the scale variation in a CNN-based detection system in terms of both efficiency and accuracy, we are inspired by the fast feature pyramid work proposed by Dollár et al. [7], where the detection system is designed for pedestrian detection using hand-crafted features. It is found that image gradients across scales can be predicted based on natural image statistics. They showed that dense feature pyramid can be efficiently constructed on top of coarsely sampled feature pyramids. In this paper, we extend the spirit of fast feature pyramid to CNN and go a few steps further. Our solution to the feature pyramid in CNN descends from the observations of modern CNN based detectors, including Faster-RCNN [27], R-FCN [4], SSD [21], YOLO [26] and STN [2], where feature maps are first computed and the detection results are decoded from the maps afterwards. However, the computation cost of generating feature maps becomes a bottleneck for methods [2, 28] using multi-scale testing and it seems not to be a neat way of addressing the scale variation problem.

To this end, our philosophy of designing an elegant detection system is that we calculate the feature pyramid *once* only, and only through that pyramid can we *approximate* the rest feature pyramids on other scales. The intuition is illustrated in Fig. 1(c). In this work, we propose a recurrent scale approximation (RSA, see Fig. 3) unit to achieve the goal aforementioned. The RSA unit is designed to be plugged at some specific depths in a network and to be fed with an initial feature map on the largest scale. The unit convolves the input in a recurrent manner to generate the prediction of the feature map that is half the size of the input. Such a scheme could feed the network with input on one scale only and approximate the rest features on smaller scales through a learnable RSA unit - a balance considering both efficiency and accuracy.

We propose two more schemes to further save the computational budget as well as improve the detection performance under the RSA framework. The first is a scale-forecast network to globally predict potential scales for a novel image and we compute feature pyramids for just a certain set of scales based on the prediction. There are only a few scales of objects appearing in the image and hence most of the feature pyramids correspond to the background, indicating a redundancy if maps on all levels are computed. The second is a landmark retracing network to retrace the location of the regressed landmarks in the preceding layers and generate a confidence score for each landmark based on the landmark feature set. The final score of identifying

a face within an anchor is thereby revised by the LRN network. Such a design could alleviate false positives due to the accumulated error in the RSA unit.

The pipeline of our proposed algorithm is shown in Fig. 2. The three components can be incorporated into a unified CNN framework and trained end-to-end. Experiments show that our approach is superior against other state-of-the-arts in face detection and achieves reasonable results for object detection.

To sum up, our contributions in this work are as follows:

1) We prove that deep CNN features for an image can be approximated from different scales using a portable recurrent unit (RSA), which fully leverages efficiency and accuracy.

2) We propose a scale-forecast network to predict valid scales of the input, which further accelerates the detection pipeline.

3) We devise a landmark retracing network to utilize landmark information to enhance the accuracy in face detection.

### 2. Related work

Multi-shot by single-scale detector. A single-scale detector detects the target on a typical scale and cannot handle features on other scales. An image pyramid is thus formulated and each level in the pyramid is fed into the detector. Such a framework appeared in pre-deep-learning era [3, 9] and usually involves hand-crafted features, *e.g.*, HOG [5] or SIFT [24], and some classifier like Adaboost [30], to verify whether context in each scale contains a target object. Recently, some CNN based methods [16, 28] also employ such a spirit to predict the objectness and class within a sliding window in each scale. In this way, the detector only handle features in a certain range of scale and the variance is taken over by the image pyramid, which could reduce the fitting difficulty for detector but potentially increase the computational cost.

Single-shot by multi-scale detector. A multi-scale detector takes one shot for the image and generates detection results aross all scales. RPN [27] and YOLO [26] has fixed size of the input scale, and proposals for all scales are generated in the final layer by using multiple classifiers. However, it is not easy to detect objects in various scales based on the final feature map. Liu et al. [21] resolved the problem via a multi-level combination of predictions from feature maps on different scales. And yet it still need a large model for large receptive field for detection. Other works [17, 20] proposed to merge deep and shallow features in a conv/deconv structure and to merge boxes for objects from different scales. These methods are usually faster than the single-scale detector since it only takes one shot for image, but the large scale invariance has to be learned by an expensive feature classifier, which is unstable and heavy.

**Face detection.** Recent years have witnessed a performance boost in face detection, which takes advantage of the

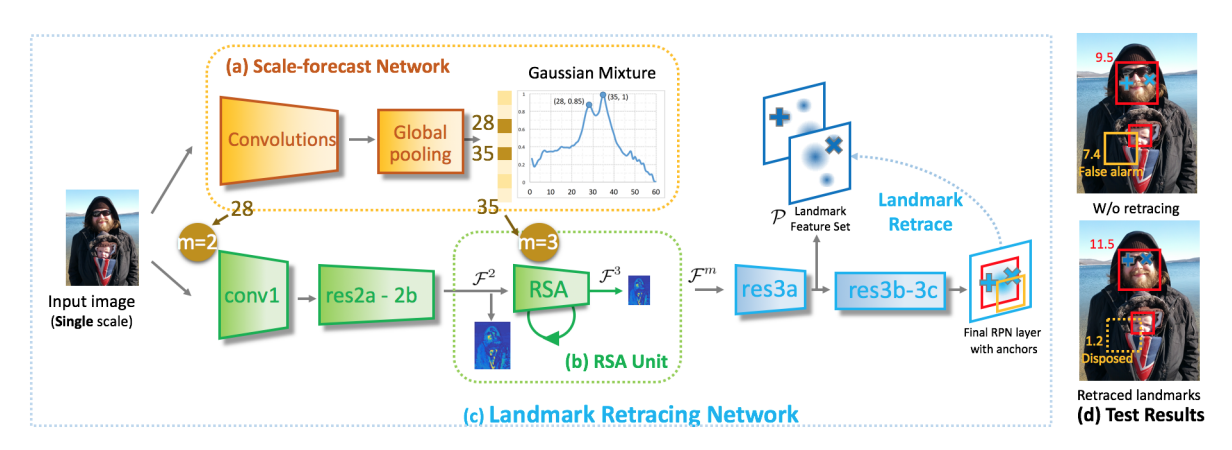


Figure 2. Pipeline of our proposed algorithm. (a) Given an image, we predict potential scales from the scale-forecast network and group the results in six main bins ( $m=0,\cdots,5$ ). (b) RSA unit. The input is resized based on the smallest scale (corresponding to the biggest feature map) and the feature maps on other scales are predicted directly from the unit. (c) Given predicted maps, LRN performs landmark detection in a RPN manner. The landmarks can *trace back* locations via regression to generate individual confidence regarding the existence of the landmark. (d) Due to the retracing mechanism, the final score of detecting a face is revised by the confidence of landmarks, which can effectively dispose of false positives.

development in fully convolutional network [8, 19, 31, 35]. Multi-task RPN is applied [2, 12, 25, 29] to generate face confidence and landmarks together. Both single-scale and multi-scale strategies are introduced in these methods. For example, Chen *et. al* [2] propose a supervised spatial transform layer to utilize landmark information and thus enhance the quality of detector by a large margin.

# 3. Our Algorithm

In this section, we depict each component of our pipeline (Fig. 2) in details. We first devise a scale-forecast network to predict potential scales of the input; the RSA unit is proposed to learn and predict features on smaller scales based on the output of the scale-forecast network; the image is fed into the landmark retracing network to detect faces of various sizes, using the scale prediction in Section 3.1 and approximation in Section 3.2. The landmark retracing network stated in Section 3.3 can retrace back features of regressed landmarks and generate individual confidence of each landmark to revise the final score of detecting a face. At last, we discuss the superiority of our algorithm's design over other alternatives in Section 3.4.

### 3.1. Scale-forecast Network

We propose a scale-forecast network (see Fig. 2(a)) to predict the possible scales of faces given an input image of fixed size. The network is a half-channel version of ResNet-18 with a global pooling at the end. The output of this network is a probability vector of B dimensions, where B=60 is the predefined number of scales. Let  $\mathcal{B}=\{0,1,\cdots,B\}$  denote the scale set, we define the mapping from a face size x, in the context of an image being

resized to longer dimension 2048, to the index b in  $\mathcal{B}$  as:

$$b = 10(\log_2 x - 5). \tag{1}$$

For example, if the face has size of 64, its corresponding bin index  $b=10^2$ . Prior to being fed into the network, an image is first resized with the longer dimension equal to 224. During training, the loss of our scale-forecast network is a binary multi-class cross entropy loss:

$$\mathcal{L}^{SF} = -\frac{1}{B} \sum_{b} p_b \log \hat{p_b} + (1 - p_b) \log(1 - \hat{p_b}), \quad (2)$$

where  $p_b$ ,  $\hat{p}_b$  are the ground truth label and prediction of the b-th scale, respectively. Note that the ground truth label for the neighbour scales  $b_i$  of an occurring scale  $b*(p_{b*}=1)$  is not zero and defined as the Gaussian sampling score:

$$p_{b_i} = \operatorname{Gaussian}(b_i, \mu, \sigma), b_i \in \mathbb{N}(b*)$$
 (3)

where  $\mu, \sigma$  are hyperparameters in the Gaussian distribution and  $\mathbb{N}(\cdot)$  denotes the neighbour set. Here we use  $\pm 2$  as the neighbour size and set  $\mu, \sigma$  to b\*,  $1/\sqrt{2\pi}$ , respectively. Such a practice could alleviate the difficulty of feature learning in the discrete distribution between occurring scales (1) and non-occurring ones (0).

For inference, we use the Gaussian mixture model to determine the local maximum and hence the potential occurring scales. Given observations x and parameterized by  $\theta$ , we can decompose the distribution into K mixture components:

$$p(\boldsymbol{\theta}|\boldsymbol{x}) = \sum_{i=1}^{K} \phi_i \mathcal{N}(\boldsymbol{\mu}_i, \boldsymbol{\Sigma}_i), \tag{4}$$

 $<sup>^2\</sup>mathrm{Here}$  we assume the minimum and maximum face size is 32 and 2048, respectively, if the longer dimension of an image is resized to 2048. In exponential expression, the face size is divided into six main bins from  $2^5=32$  to  $2^{11}=2048$ , of which denotation we will use later.

where the *i*-th component is characterized by Gaussian distributions with weights  $\phi_i$ , means  $\mu_i$  and covariance matrices  $\Sigma_i$ . Here we use  $K=\{1,...,6\}$  to denote selected scale numbers of six main scales from  $2^5$  to  $2^{11}$  and the selection of scales is determined by thresholding  $\phi_i$  of each component. Finally the best fitting model with specific K is used.

# 3.2. Recurrent Scale Approximation (RSA) Unit

The recurrent scale approximation (RSA) unit is devised to predict feature maps on smaller scales given a map on the largest scale. Fig. 2 depicts the RSA unit. The network architecture follows a similar build-up of the residual network [13], where we reduce the number of channels in each convolutional layer to half of the original version to leverage time efficiency. The structure details are shown in Section 4.1. Given an input image  $\mathcal{I}$ , we denote  $\mathcal{I}^m$  as the downsampled result of the image with a ratio of  $1/2^m$ , where  $m \in \{0,\cdots,M\}$  is the downsample level and M=5. Note that  $\mathcal{I}^0$  is the original image. Therefore, there are six scales in total, corresponding to the six main scale range defined in the scale-forecast network (see Section 3.1). Given an input image  $\mathcal{I}^m$ , we define the output feature map of layer res2b as:

$$f(\mathcal{I}^m) = \mathcal{G}^m,\tag{5}$$

where  $f(\cdot)$  stands for a set of convolutions with a total stride of 8 from the input image to the output map. The set of feature maps  $\mathcal{G}^m$  on different scales serve as the ground truth supervision of the recurrent unit.

The RSA module  $RSA(\cdot)$  takes as input the feature map of the largest scale  $\mathcal{G}^0$  at first, and repeatedly outputs a map with half the size of the input map:

$$h^{(0)} = \mathcal{F}^0 = \mathcal{G}^0,$$
  
$$h^{(m)} = \text{RSA}(h^{(m-1)}|\boldsymbol{w}) = \mathcal{F}^m.$$
 (6)

where  $\mathcal{F}^m$  is the resultant map after rolling out m times, w are the weights in the RSA unit. The RSA module has four convolutions with a total stride of 2 (1,2,1,1) and their kernal sizes are (1,3,3,1). The loss is therefore the  $l_2$  norm between prediction  $\mathcal{F}^m$  and supervision  $\mathcal{G}^m$  across all scales:

$$\mathcal{L}^{RSA} = \frac{1}{2M} \sum_{m=1}^{M} \left\| \mathcal{F}^m - \mathcal{G}^m \right\|^2.$$
 (7)

The gradients in the RSA unit are computed as:

$$\frac{\partial \mathcal{L}^{RSA}}{\partial \boldsymbol{w}_{xy}} = \sum_{m} \frac{\partial \mathcal{L}^{RSA}}{\partial h^{(m)}} \cdot \frac{\partial h^{(m)}}{\partial \boldsymbol{w}_{xy}},$$

$$= \frac{1}{M} \sum_{m} (\mathcal{F}^{m} - \mathcal{G}^{m}) \cdot \mathcal{F}_{xy}^{m-1}, \qquad (8)$$

where x, y are the spatial index in the feature map<sup>3</sup>.

The essence behind our RSA unit is to derive a mapping  $RSA(\cdot) \mapsto f(\cdot)$  to constantly predict lower-scale features based on current map instead of forwarding the network with different scale inputs multiple times. In a non-strict mathematical expression, we have:

$$\lim_{0 \to m} \mathrm{RSA}\big(h^{(m-1)}\big) = f(\mathcal{I}^m) = \mathcal{G}^m,$$

to indicate the functionality of RSA: an approximation to  $f(\cdot)$  from the input on largest scale 0 to its desired level m. The computation cost to generate feature map  $\mathcal{F}^m$  using RSA is much fewer than that by resizing the image and feeding into the network (i.e.,  $f(\mathcal{I}^m)$  through conv1 to res2b; see quantitative results in Section 4.4).

During inference, we first have the possible scales of the input from the scale-forecast network. The image is then resized accordingly to the extent that the smallest scale (corresponding to the largest feature map) is resized to the range of [64,128]. The feature maps on other scales are thereby predicted by the output of RSA unit via Eqn (6). Fig. 3 depicts a rolled-out version of RSA to predict feature maps of smaller scales compared with the ground truth. We can observe from both the error rate and predicted feature maps in each level that RSA is capable of approximating the feature maps on smaller scales.

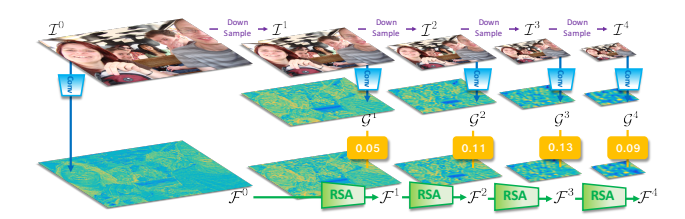


Figure 3. RSA by rolling out the learned feature map on smaller scales. The number in the orange box indicates the average mean squared error between ground truth and RSA's prediction.

### 3.3. Landmark Retracing Network

In face detection task, as illustrated in Fig. 2, the landmark retracing network (LRN) is designed to adjust the confidence of identifying a face and to dispose of false positives by learning individual confidence of each regressed landmark. Instead of directly using the ground truth location of landmarks, we formulate such a feature learning of landmarks based on the regression *output* of landmarks in the final RPN layer.

Specifically, given the feature map  $\mathcal{F}$  on a specific scale from RSA (drop m for brevity), we first feed it into the res3a layer. There are two branches at the output: one

<sup>&</sup>lt;sup>3</sup>For brevity of discussion, we ignore the spatial weight sharing of convolution here. Note that the weight update in  $\boldsymbol{w}_{xy}$  also includes the loss from the landmark retracing network.

is the landmark feature set  $\mathcal{P}$  to predict the individual score of each landmark in a spatial context. The number of channels in the set equals to the number of landmarks. Another branch is continuing the standard RPN [27] pipeline (res3b-3c) which generates a set of anchors in the final RPN layer. Let  $p_i = [p_{i0}, p_{i1}, \cdots, p_{ik}, \cdots]$  denote the classification probability in the final RPN layer, where k is the class index and i is the spatial location index on the map;  $t_{ij}$  denote the regression target (offset defined in [10]) of the j-th landmark in the i-th anchor, where  $j = \{1, \cdots, 5\}$  is the landmark index. Note that in face detection task, we only have one anchor so that  $p_i$  contains one element. In the traditional detection-to-landmark formulation, the following loss, which consists of two heads (i.e., classification and regression), is optimized:

$$\sum_{i} -\log p_{ik^*} + \delta(k^*) \mathcal{S}(\boldsymbol{t}_i - \boldsymbol{t}_i^*),$$

where  $\delta(\cdot)$  is the indicator function;  $k^*$  denotes the correct label of anchor i and we have only two classes here (0 for background, 1 for positive);  $t_i^*$  is the ground truth regression target and  $\mathcal{S}(\cdot)$  is the smoothing  $l_1$  loss defined in [10].

However, as illustrated in Fig. 2(c), using the confidence of anchor  $p_{ik^*}$  alone could have false positives in some cases, which leads us to the intuition that taking advantage of the landmark features based on the regression output. The revised classification output,  $p_{ik^*}^{trace}(t_{ij})$ , now both considers the feature in the final RPN layer as well as those in the landmark feature set:

$$p_{ik^*}^{trace}(t_{ij}) = \begin{cases} p_{i0}, & k^* = 0, \\ \max_{pool}(p_{i1}, p_{ij}^{land}), & k^* = 1, \end{cases}$$
(9)

where  $p_{ij}^{land}$  is the classification output of point j from the landmark feature set  $\mathcal P$  and it is determined by the regression output:

$$p_{ij}^{land} = \mathcal{P}(r(t_{ij})), \tag{10}$$

where  $r(\cdot)$  stands for a mapping from the regression target to the spatial location on map  $\mathcal{P}$ . To this end, we have the revised loss for our landmark retracing network:

$$\mathcal{L}^{LRN} = \sum_{i} \left[ -\log p_{ik^*}^{trace}(t_{ij}) + \delta(k^*) \sum_{j} \mathcal{S}(t_{ij} - t_{ij}^*) \right]. \tag{11}$$

Apart from the detection-to-landmark design as previous work did, our retracing network also fully leverages the feature set of landmarks to help rectify the confidence of identifying a face. This is achieved by utilizing the regression output  $t_{ij}$  to find the individual score of each landmark on the preceding feature map  $\mathcal{P}$ . Such a scheme is in a landmark-to-detection spirit.

Note that the landmark retracing network is trained endto-end with the RSA unit stated previously. The anchor associated with each location i is a square box and of fixed size  $64\sqrt{2}$ . Only the anchor is a positive sample does the landmark retracing operation is performed. The base landmark location with respect to the anchor is determined by the average location of all faces in the training set. During test, LRN is fed with feature maps on various scales and it treats each scale individually. The final detection is generated after doing NMS among results from multi-scales.

#### 3.4. Discussion

Comparison to RPN. The region proposal network [27] takes a set of predefined anchors on different sizes as input and conducts a similar detection pipeline. Anchors in RPN vary in size to meet the multi-scale training constraint. During one iteration of update, it has to feed the whole image of different sizes (scales) from the start to the very end of the network. In our framework, we resize the image *once* to make sure at least one face falls into the size of [64, 128], thus enforcing the network to be trained within a certain range of scales. In this way, we can only use one anchor of fixed size. The multi-scale spirit is embedded by a RSA unit, directly predicting the feature maps on smaller scales. Such a scheme saves parameters significantly and could be considered as a 'semi' multi-scale training and 'fully' multi-scale test.

Prediction-supervised or GT-supervised in landmark feature sets. Another comment in our framework is the supervision knowledge used in training the landmark features  $\mathcal{P}$ . The features are learned using the prediction output of regression targets  $t_{ij}$  instead of the ground truth targets  $t_{ij}^*$ . In our preliminary experiments, we find if  $p_i^{land} \sim t_i^*$ , the activation in the landmark features could be much prohibited due to the misleading regression output by  $t_{ij}$ ; however, if we loose learning constraint and tolerate activations within a certain range of misleading locations, i.e.,  $p_i^{land} \sim t_i$ , the performance could boost in great extent. Using the prediction of regression as supervision in the landmark feature learning makes sense since: (a) we care about the activation (classification probability) of each landmark, instead of each's accurate location; (b)  $t_i$  and  $p_i^{land}$  shares similar learning workflow and thus the location of  $t_i$  could better match the activation  $p_i^{land}$  in  $\mathcal{P}$ .

# 4. Experiments

In this section we first conduct the ablation study to verify the effectiveness of each component in our method and compare exhaustively with the baseline RPN [27]; then we compare our algorithm with state-of-the-arts in face detection and object detection on four popular benchmarks.

### 4.1. Setup and Implementation Details

Annotated Faces in the Wild (AFW) [37] contains 205 images for evaluating face detectors' performance. However, some faces are missed in the annotations and could

trigger the issue of false positives, we relabel those missing faces and report the performance difference in both cases. Face Detection Data Set and Benchmark (FDDB) [14] has 5,171 annotated faces in 2,845 images. It is larger and more challenging than AFW. Multi-Attribute Labelled Faces (MALF) [32] includes 5,250 images with 11,931 annotated faces collected from the Internet. The annotation set is more clean than that on AFW and it is the largest benchmark for face detection.

Our training set has 184K images, which contains 171K images collected from internet and 12.9K images from the training split of Wider Face Dataset [33]. All faces are labelled with bounding boxes and five landmarks. The structure of our model is a shallow version of the ResNet [13] where the first seven ResNet blocks are used, i.e., from conv1 to res3c. We use this model in scale-forecast network and LRN. The number of channels are set unanimously to half of the original ResNet model, for the consideration of time efficiency. We first train the scale-forecast network and the output of predicted scales are used to launch RSA unit and LRN afterwards. Note that the whole system (R-SA+LRN) is trained end-to-end and the model is trained from scratch without resorting to a pretrain model since the number of channels is halved. In all experiments, we balance the ratio of the positive and the negative to be 1:1. The batch size is 4; base learning rate set to 0.001 with a decrease of 6% every 10,000 iteration. The maximum training iteration is 1,000,000. We use stochastic gradient descent as the optimizer.

## 4.2. Performance of Scale-forecast Network

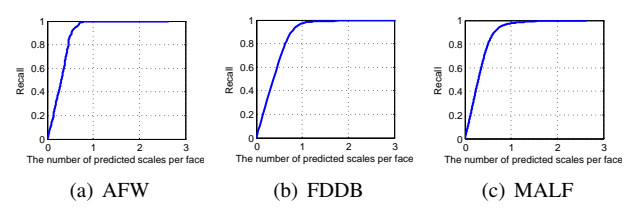


Figure 4. Recall v.s. the number of predicted scales per face on three benchmarks. Our scale-forecast network almost recalls all scales when the number of predicted scale per face is 1.

The scale-forecast network is of vital importance to the computational cost and accuracy in the networks afterwards. Fig. 4 reports the overall recall under different number of predicted scales on three benchmarks. Since the number of faces and the number of potential scales in the image vary across datasets, we use *the number of predicted scales per face*  $(x, \text{ total predicted scales over total number of faces) and a global$ *recall* $<math>(y, \text{ correct predicted scales over all ground truth scales) to be the evaluation metric. We can observe from the results that our trained scale network can recall almost 99% at <math>x=1$ , meaning on average we only need to generate less than two prediction per image and we

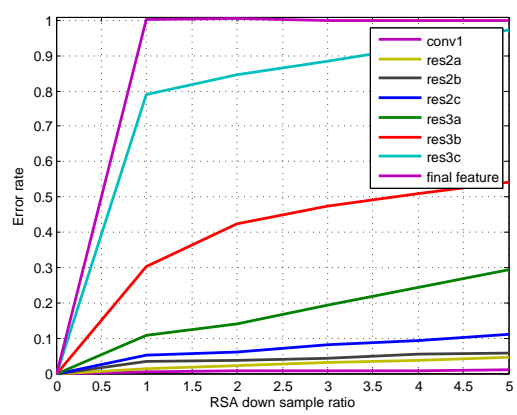


Figure 5. Investigation on the source layer to branch out RSA unit. For each case, we report the error rate v.s. the level of downsampling ratio in the unit. We can conclude that the deeper RSA is branched out, the more inferior the feature approximation on smaller scales will be.

can retrieve all faces' scales. Based on this prior knowledge, during inference, we set the threshold for predicting potential scales of the input as to the extent that it has approximately two predictions.

## 4.3. Ablative Evaluation on RSA Unit

Fig. 5 investigates the effect as to which layer we should append the RSA unit after. For each case, the error rate between the ground truth and corresponding prediction is computed. We define the error rate (ER) on level m as:

$$ER^{m} = \frac{1}{N} \sum_{i}^{N} ((\mathcal{F}^{(m)} - \mathcal{G}^{(m)})./\mathcal{G}^{(m)})^{2}, \quad (12)$$

where './' implies an element-wise division between maps; N is the total number of samples. We use a separate validation set to conduct this experiment. The image is first resized to longer dimension being 2048 and the RSA unit predicts six scales defined in Section 3.1 (1024, 512, 256, 128 and 64). Ground truth maps are generated accordingly as we iteratively resize the image (see Fig. 3). There are two remarks regarding the result:

First, feature depth matters. Theoretically RSA can handle all scales of features in a deep CNN model and therefore can be branched out at any depth of the network. However, results from the figure implies that as we plug RSA at deeper layers, its performance decades. Since features at deeper layers are more sparse and abstract, they barely contain information for RSA to approximate the features on smaller scale. For example, in case final feature which means RSA is plugged at the final convolution layer after res3c, the error rate is almost 100%, indicating RSA's incapability of handling the deficient information in this layer. Things get better in shallower cases.

However, the computation cost of RSA at shallow layers

Table 1. The proposed algorithm is more computational efficient and accurate by design than baseline RPN. The theoretical operations of each component is provided, denoted as 'Opts. (VGA input)' below. The minimum operation in each component means only the scale-forecast network is used where no face appears in the image; and the maximum operation indicates the amount where faces appear in all scales. The actual runtime comparison between ours and baseline RPN is reported in Table 2.

Component	Scale-forecast	RSA	LRN	Total Pipeline	Baselin	ne RPN
Structure	tiny ResNet-18	4-layer FCN	tiny ResNet-18	95.67M to 1.5G	single anchor	multi anchors
Opts. (VGA input)	95.67M	0 to 182.42M	0 to 1.3G		1.72G	1.31G
AP@AFW	-	-	-	99.96%	99.90%	98.29%
Recall@FDDB1%fpi	-	-	-	91.92%	90.61%	86.89%
Recall@MALF1%fpi	-	-	-	90.09%	88.81%	84.65%

is much more than that at deeper layers, since the stride is smaller and the input map of RSA is thus larger. The path on one-time forward from image to the input map right before RSA is shorter; and the rolling out time increases accordingly. Therefore, the trade-off is that we want to plug RSA at shallow layers to ensure a low error rate and at the same time, to save the computational cost. In practice we choose case res2b to be the location where RSA is branched out. The most computation lies before layer res2b and it has an endurable error rate of 3.44%. We use such a setting throughout the following experiments.

Second, butterfly effect exists. For a particular case, as the times of the recurrent operation increases, the error rate goes up due to the cumulative effect of rolling out the predictions. For example, in case res2b, the error is 3.44% at level m=1 and goes slightly worse to 5.9% after rolling out five times. Such an increase is within the tolerance of the system and still suffices the task of face detection.

## 4.4. Our Algorithm vs. Baseline RPN

We compare our model (denote as RSA+LRN), a combination of RSA unit plus the landmark retracing network, with the region proposal network (RPN) [27]. In the first setting, we use the original RPN with multiple anchors (denote as RPN\_m) to detect faces of various scales. In the second setting, we modify the number of anchors to one single anchor (denote as RPN\_s); the anchor can only detect faces in the range from 64 to 128 pixels. To capture all faces, it needs to take multiple shots in an image pyramid spirit. The network structure of baseline RPN and our L-RN both descends from ResNet-18 [13]. Anchor sizes in the first setting RPN\_m is  $32\sqrt{2}, 64\sqrt{2}, \cdots, 1024\sqrt{2}$  and they are responsible for detecting faces in the range of  $[32, 64), [64, 128), \dots, [1024, 2048],$  respectively. In the second setting RPN\_s, we first resize the image length to  $64, 256, \dots, 2048$ , then test each scale one-by-one and merge all results through NMS [1].

Table 1 shows the theoretical computation cost and test performance of our algorithm compared with baseline RP-N. We can observe that RPN\_s needs six shots for the same image during inference and thus the computation cost is much larger than ours or RPN\_m; Moreover, RPN\_m per-

Table 2. Test runtime (ms per image) of RSA compared with RPN on three benchmarks. We conduct experiments of each case five times and report the average result to avoid system disturbance.

Speed	LRN+RSA	LRN	RPN_s	<b>RPN</b> _m
AFW	13.95	28.84	26.85	18.92
FDDB	11.24	27.10	25.01	18.34
MALF	16.38	29.73	27.37	19.37
Average	14.50	28.78	26.52	18.99

forms worse than the rest two based on two reasons: First, the receptive field is less than 500 and therefore it cannot see the context of faces larger than 500 pixels; second, it is hard for the network (model capacity much less than the original ResNet [13]) to learn the features of faces in a wide scale range from 32 to 2048.

Table 2 depicts the runtime comparison during test. The third column LRN means without using the RSA unit. Our method can be run fast enough compared with other counterparts due to two reasons. First, there are often one or two valid scales in the image, and the scale-forecast network can automatically select some particular scales, and ignore all the other invalid ones in the multi-scale test stage; second, the input of LRN descends from the output of RSA to predict feature maps on smaller scales; it is not necessary to compute feature maps of multiple scales in a multi-shot manner as does in RPN\_m.

### 4.5. Face Detection

Fig. 7 shows the comparison against other approaches on three benchmarks. On AFW, our algorithm achieves an AP of 99.17% using the origin annotation and an AP of 99.96% using the revised annotation 7(c). On FDDB, RSA+LRN recalls 93.0% faces with 50 false positive 7(a). On MALF, our method recalls 82.4% faces with zero false positive 7(d). It should be noticed that the shape and scale definition of bounding box on each benchmark varies. For instance, the annotation on FDDB is ellipse while others are rectangle. To address this, we learn a transformer to fit each annotation from the landmarks. This strategy significantly enhances performance in the continuous setting on FDDB.



Figure 6. Our proposed model can detect faces at various scales, including the green annotations provided in AFW [37] as well as faces marked in red that are of small sizes and not labeled in the dataset.

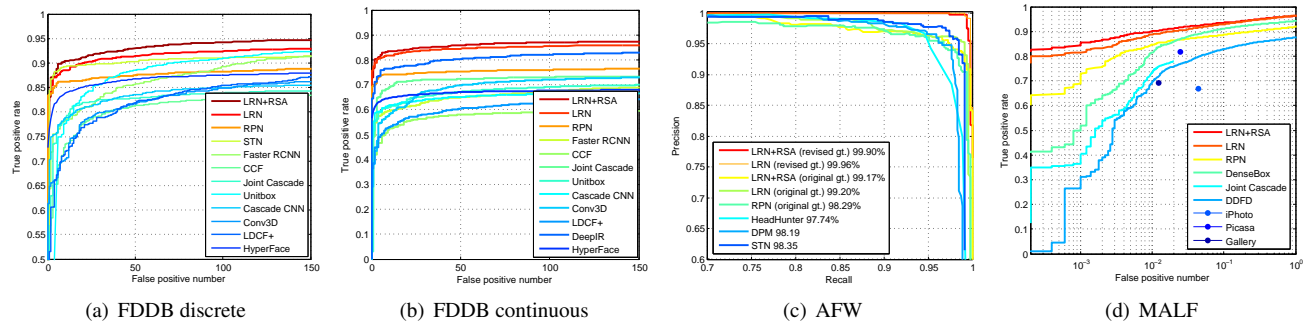


Figure 7. Comparison to state-of-the-arts on face detection benchmarks. The proposed algorithm (Scale-forecast network with RSA+LRN, tagged by LRN+RSA) outperforms against other methods by a large margin. 'revised gt.' and 'original gt.' in AFW stand for fully annotated faces by us and partially labeled annotations provided by the dataset, respectively.

Table 3. Recall (%) vs. the number of proposals and Speed (ms per image) breakdown on ILSVRC DET val2.

Recall	100	300	1000	2000	Speed
Original RPN	88.7	93.5	97.3	97.7	158 ms
Single-scale RPN	89.6	94.4	97.2	98.0	249 ms
RSA+RPN	89.1	94.4	97.2	98.0	124 ms

## 4.6. RSA on Generic Object Proposal

We now verify that the scale approximation learning by RSA unit also generalizes comparably well on the generic region proposal task. Region proposal detection is a basic stage for generic object detection task and is a more challenging problem than face detection. ILSVRC DET [6] is a challenging dataset for generic object detection. It contains more than 300K images for training and 20K images for validation. We use partial data (around 170k images) of the original training set for training, where each category could have at most 1000 samples; for test we use the val2 split [11] with 9917 images. We use the single anchor RPN with ResNet-101 to be the baseline. RSA unit is set after res3b3. The anchors are of size  $128\sqrt{2}$  squared,  $128 \times 256$  and  $256 \times 128$ . During training, we randomly select one object and resize the image to the extent where the object is rescaled to [128, 256]. Scale-forecast network is also introduced to predict the longer dimension of objects in the image.

Recalls under different number of proposals are shown in

Table 3. The original RPN setting has 18 anchors with 3 aspect ratios and 6 scales. RPN+RSA reduces around 61.05% less computation cost compared with the single-scale RPN, without loss of recall when the number of boxes is over 100. And it is more efficiency and recalls more objects compared with original RPN. Our model and the single-anchor RPN both perform better than the original RPN. This observation is in accordance with the conclusion in face detection. Overall, our scheme of using RSA plus LRN competes comparably with the standard RPN method in terms of computation efficiency and accuracy.

### 5. Conclusion

In this paper, we prove that deep CNN features for an image can be approximated from a large scale to smaller scales by the proposed RSA unit, which can significantly accelerate face detection and achieve comparable results in object detection. In order to make the detector faster and more accurate, we devise a scale-forecast network for predicting the potential scales of objects. Furthermore, we use the landmark retracing network to fuse global and local scale information to enhance the predictor. Experimental results show that our algorithm achieves favourably superior against state-of-the-arts. Our future work will explore RSA on generic object detection task. Representation approximation between video frames is also an interesting issue.

### References

- [1] B. Alexe, T. Deselares, and V. Ferrari. Measuring the objectness of image windows. *IEEE Trans on PAMI*, 2012.
- [2] D. Chen, G. Hua, F. Wen, and J. Sun. Supervised transformer network for efficient face detection. In *ECCV*, pages 122– 138. Springer, 2016.
- [3] D. Chen, S. Ren, Y. Wei, X. Cao, and J. Sun. Joint cascade face detection and alignment. In *ECCV*, pages 109–122. Springer, 2014.
- [4] J. Dai, Y. Li, K. He, and J. Sun. R-fcn: Object detection via region-based fully convolutional networks. In D. D. Lee, M. Sugiyama, U. V. Luxburg, I. Guyon, and R. Garnett, editors, *Advances in Neural Information Processing Systems* 29, pages 379–387. Curran Associates, Inc., 2016.
- [5] N. Dalal and B. Triggs. Histograms of oriented gradients for human detection. In *IEEE Computer Society Conference* on Computer Vision & Pattern Recognition, pages 886–893, 2005
- [6] J. Deng, W. Dong, R. Socher, L.-J. Li, K. Li, and L. Fei-Fei. ImageNet: A Large-Scale Hierarchical Image Database. In CVPR, 2009.
- [7] P. Dollár, R. Appel, S. Belongie, and P. Perona. Fast feature pyramids for object detection. *IEEE Transactions on Pattern Analysis and Machine Intelligence*, 36(8):1532–1545, 2014.
- [8] S. S. Farfade, M. J. Saberian, and L.-J. Li. Multi-view face detection using deep convolutional neural networks. In *Pro*ceedings of the 5th ACM on International Conference on Multimedia Retrieval, pages 643–650. ACM, 2015.
- [9] P. F. Felzenszwalb, R. B. Girshick, and D. Mcallester. Cascade object detection with deformable part models. In *CVPR*. IEEE, 2010.
- [10] R. Girshick. Fast R-CNN. In ICCV, 2015.
- [11] R. Girshick, J. Donahue, T. Darrell, and J. Malik. Rich feature hierarchies for accurate object detection and semantic segmentation. In CVPR, pages 580–587, 2014.
- [12] Z. Hao, Y. Liu, H. Qin, and J. Yan. Scale-aware face detection. In CVPR 2017, 2017.
- [13] K. He, X. Zhang, S. Ren, and J. Sun. Deep residual learning for image recognition. In *CVPR*, 2016.
- [14] V. Jain and E. Learned-Miller. Fddb: A benchmark for face detection in unconstrained settings. Technical Report UM-CS-2010-009, University of Massachusetts, Amherst, 2010.
- [15] B. Leng, Y. Liu, K. Yu, X. Zhang, and Z. Xiong. 3d object understanding with 3d convolutional neural networks. *Information Sciences*, 366:188–201, 2016.
- [16] H. Li, Z. Lin, X. Shen, J. Brandt, and G. Hua. A convolutional neural network cascade for face detection. In CVPR, pages 5325–5334, 2015.
- [17] H. Li, Y. Liu, W. Ouyang, and X. Wang. Zoom out-and-in network with recursive training for object proposal. *arXiv* preprint arXiv:1702.05711, 2017.
- [18] H. Li, Y. Liu, X. Zhang, Z. An, J. Wang, Y. Chen, and J. Tong. Do we really need more training data for object localization. In *IEEE International Conference on Image Processing*, 2017.
- [19] Y. Li, B. Sun, T. Wu, and Y. Wang. Face detection with end-to-end integration of a convnet and a 3d model. In *ECCV*, pages 420–436. Springer, 2016.
- [20] T.-Y. Lin, P. Dollár, R. Girshick, K. He, B. Hariharan, and

- S. Belongie. Feature pyramid networks for object detection. *arXiv preprint arXiv:1612.03144*, 2016.
- [21] W. Liu, D. Anguelov, D. Erhan, C. Szegedy, S. Reed, C.-Y. Fu, and A. C. Berg. Ssd: Single shot multibox detector. In *ECCV*, pages 21–37. Springer, 2016.
- [22] Y. Liu, H. Li, and X. Wang. Learning deep features via congenerous cosine loss for person recognition. arXiv preprint arXiv:1702.06890, 2017.
- [23] Y. Liu, J. Yan, and W. Ouyang. Quality aware network for set to set recognition. In CVPR. 2017.
- [24] D. G. Lowe. Distinctive image features from scaleinvariant keypoints. *International journal of computer vi*sion, 60(2):91–110, 2004.
- [25] R. Ranjan, V. M. Patel, and R. Chellappa. Hyperface: A deep multi-task learning framework for face detection, landmark localization, pose estimation, and gender recognition. *arXiv* preprint arXiv:1603.01249, 2016.
- [26] J. Redmon, S. Divvala, R. Girshick, and A. Farhadi. You only look once: Unified, real-time object detection. In *Proceedings of the CVPR*, pages 779–788, 2016.
- [27] S. Ren, K. He, R. Girshick, and J. Sun. Faster R-CNN: Towards Real-Time Object Detection with Region Proposal Networks. In NIPS, 2015.
- [28] P. Sermanet, D. Eigen, X. Zhang, M. Mathieu, R. Fergus, and Y. LeCun. Overfeat: Integrated recognition, localization and detection using convolutional networks. In *ICLR*, 2014.
- [29] X. Sun, P. Wu, and S. C. Hoi. Face detection using deep learning: An improved faster rcnn approach. arXiv preprint arXiv:1701.08289, 2017.
- [30] P. Viola and M. J. Jones. Robust real-time face detection. International journal of computer vision, 57(2):137–154, 2004.
- [31] B. Yang, J. Yan, Z. Lei, and S. Z. Li. Convolutional channel features. In *Proceedings of the IEEE international conference on computer vision*, pages 82–90, 2015.
- [32] B. Yang, J. Yan, Z. Lei, and S. Z. Li. Fine-grained evaluation on face detection in the wild. In *Automatic Face and Gesture Recognition (FG)*, 11th IEEE International Conference on. IEEE, 2015.
- [33] S. Yang, P. Luo, C. C. Loy, and X. Tang. Wider face: A face detection benchmark. In CVPR, 2016.
- [34] F. Yu, W. Li, Q. Li, Y. Liu, X. Shi, and J. Yan. Poi: Multiple object tracking with high performance detection and appearance feature. In *ECCV*, pages 36–42. Springer International Publishing, 2016.
- [35] J. Yu, Y. Jiang, Z. Wang, Z. Cao, and T. Huang. Unitbox: An advanced object detection network. In *Proceedings of the 2016 ACM on Multimedia Conference*, pages 516–520. ACM, 2016.
- [36] X. Zeng, W. Ouyang, J. Yan, H. Li, T. Xiao, K. Wang, Y. Liu, Y. Zhou, B. Yang, Z. Wang, et al. Crafting gbd-net for object detection. arXiv preprint arXiv:1610.02579, 2016.
- [37] X. Zhu and D. Ramanan. Face detection, pose estimation, and landmark localization in the wild. In CVPR, pages 2879– 2886, 2012.